J. Cent. South Univ. (2022) 29: 3422−3435
DOI: https://doi.org/10.1007/s11771-022-5091-9

Springer

Direct microwelding of dissimilar glass and Kovar alloy without optical contact using femtosecond laser pulses

JI Chang-hao(纪昌豪)[1], HUANG Yu-jia(黄裕佳)[2], CHEN Xu(陈旭)[1],
JIANG Ji-yan(蒋佶岩)[1], GUO Zhi-jun(郭志俊)[1], LONG Yu(龙雨)[1]*

1. Institute of Laser Intelligent Manufacturing and Precision Processing, School of Mechanical Engineering, Guangxi University, Nanning 530004, China;
2. Han's Laser Technology Industry Group Co., Ltd., Shenzhen 518057, China

© Central South University 2022

Abstract: In the current microwelding process using femtosecond (fs) laser between dissimilar materials, surface polishing and pressure assistance, so-called optical contact, are believed necessary. In this paper, direct welding of soda lime glass and Kovar alloy using a fs laser is investigated to overcome the limit of optical contact. The processing of fs laser welding is comprehensively studied by varying the laser power, welding velocity and the number of welding. The shear joining strength is as high as 2 MPa. The cross-section of glass-Kovar alloy joints, the elemental diffusion and the fracture behavior of welded joints were studied. The results show that the fs laser irradiates the surface of Kovar alloy, micron/nanometer-sized metal particles are generated. These particles perform the role as an adhesive part in the welding process. It is believed that the Si atoms diffuses to Kovar alloy from the glass and partially replaces the Fe^{2+} ions on the surface of Kovar alloy, indicating that the mixing and interdiffusion of materials have occurred during the welding process. Finally, the welded sample was tested and has excellent water resistance and sealing property. Furthermore, to justify that this method can be applied to other stack ups, the glass-copper, the glass-Al6063 and sapphire-ceramic are also welded together. This work greatly simplifies the fs laser microwelding process and promotes its industrial applications, such as optoelectronic devices, medical devices and MEMS.

Key words: femtosecond laser; microwelding; glass; Kovar alloy; optical contact

Cite this article as: JI Chang-hao, HUANG Yu-jia, CHEN Xu, JIANG Ji-yan, GUO Zhi-jun, LONG Yu. Direct microwelding of dissimilar glass and Kovar alloy without optical contact using femtosecond laser pulses [J]. Journal of Central South University, 2022, 29(10): 3422−3435. DOI: https://doi.org/10.1007/s11771-022-5091-9.

1 Introduction

Glass is prone to fracture due to their inherent brittleness and low ductility, and limited in engineering applications, although exhibiting great properties such as high strength, hardness, wear resistance, excellent corrosion resistance and optical properties [1]. Considering metal has superior mechanical property and ductility [2], the glass-metal compound components have met great demands in the fields of sensors, medical and semiconductor devices, vacuum-sealed connectors, micro electro mechanical system (MEMS), etc [3−7]. By far, the traditional methods of joining glass and metal include adhesive bonding, anodic bonding, solid phase bonding, and fusion

Foundation item: Project(GKZY2119502) supported by the Special Funds for Local Scientific and Technological Development guided by the Central Government, China; Project(JGY2021001) supported by the Innovation Project of Guangxi Graduate Education, China
Received date: 2022-03-09; **Accepted date:** 2022-04-28
Corresponding author: LONG Yu, PhD, Professor; E-mail: longyu@gxu.edu.cn; ORCID: https://orcid.org/0000-0001-7486-3675

microwelding. However, these methods have drawbacks, such as creep, contamination, aging, and low accuracy [8].

The technique of femtosecond (fs) laser microwelding has quickly become a popular research topic in recent years [9 − 11]. The fs-laser could weld transparent similar/dissimilar materials without inserting an absorbent intermediate layer and weld dissimilar transparent materials with different thermal coefficient [12 − 13]. In this technique, the focused fs-laser can directly melt not only metal but also glass through nonlinear absorption. Glass materials are hard and brittle, and have low thermal conductivity relative to metal materials. When heated unevenly, it is prone to cracking due to internal stress. Fs-laser can prevent this phenomenon. This possibly reduces unwanted thermal effects.

Previous study showed that in ultrafast laser welding, RICHTER et al [14] established that in order to prevent the plasma from escaping at the interface, and the gap is limited by no more than about 100 − 500 nm. In most of the research works, in order to realize a close contact between two pieces of materials, clamps and materials surface polishing were usually thought to be a necessary component when glass and metal are welded by ultrafast laser. OZEKI et al [15] successfully implemented the welding of glass and copper by fs-laser using clamps to provide pressure assistance. QUINTINO et al [16] used a fs-laser to successfully direct weld NiTi sheet and glass. CARTER et al [17] reported their findings of systematic analysis and comparison of picosecond (ps) laser microwelding of industry related Al6082 parts to SiO_2 and BK7. In their paper, a pneumatic clamp was used to ensure close contact against the plasma escape; without the clamp, otherwise, the formation of the plasma in the melting process would be difficult when there exists any big gap during welding. LAFON et al [18] reported that direct welding between glass and copper, sapphire and aluminum using ultrafast laser after polishing the materials and providing pressure assistance with fixtures to provide optical contact between the two materials. In all of those research, one common challenge to ultrafast laser microwelding is a prerequirement for optical contact or partial-optical contact between the dissimilar materials. Samples were stacked with a clamp to reduce the gap between glass and metal. However, when samples are pressed, residual stress was introduced on the welding interface, causing cracks and inconveniences that hinder the welding processes. Interestingly, ZHANG et al [19] implemented the direct welding of alumina silicate glass and metal for the first time without any pressure assistance, using a fs laser. However, polishing of the sample surface was still used in their study, which was very time-consuming to use mechanical polishing to achieve the required surface quality. And the pretreatment polishing process is significantly complicated when facing a large area (several hundred square millimeters or larger). Therefore, it is necessary to simplify the glass-metal microwelding process by investigating the effect of non-optical contact during the process.

In this paper, direct microwelding of soda lime glass and Kovar alloy by a 1030 nm fs laser is accomplished without surface polishing and pressure assistance. Firstly, the influence of the laser power, welding velocity, and the number of welding on shear joining strength were studied experimentally. Then, the cross-section of glass-Kovar alloy joints, the elemental diffusion and the fracture behavior of welded joints were studied by optical microscope (OM), scanning electron microscopy (SEM), energy dispersive spectrometry (EDS), to provide a preliminary exploration for the interface evolution and joining mechanism. The mechanism of microwelding and formation of plasma escape zone was discussed. Finally, the welded sample is tested for water sealing performance. This work aims to simplify the welding process by eliminating the need for fixture design and material polishing, which is helpful to provide a reference for the industrial application of ultrafast laser welding technology, thus improving process efficiency and automation.

2 Materials and methods

2.1 Materials

The glass and metal used in the experiment are soda lime glass and Kovar alloy, respectively. The main chemical compositions of the Kovar alloy are 53% Fe, 29% Ni and 17% Co. The soda lime glass, one of the silicate glasses, is mainly composed of SiO_2 (about 72%), Na_2O (about 15%) and CaO

(about 9%), and a small amount of Al_2O_3, MgO, K_2O, etc. The metal samples with the size of 60 mm×60 mm×0.5 mm were cleaned with acetone and anhydrous ethanol before use, without any additional polishing. Soda lime glass with the dimension of 30 mm×15 mm×1 mm was used, without any additional polishing. Simultaneously, the glass and metal are washed clean with acetone and absolute ethanol (the purity of $CH_3CH_2OH \geqslant$ 99.7%) to guarantee that their surfaces are free of dusty fingerprints and other unclean residues. In this paper, acetone and absolute ethanol are used to clean glass and Kovar alloy, so that there are no visible impurities and defects on the surface, without carrying out polishing treatment. The glass was stacked onto the metal surface with no need of pressure assistance. After the glass and Kovar alloy are cleaned, the initial state of the surface is characterized by a optical microscope. Figures 1(a_1) and (b_1) present an optical image of the initial surface states of Kovar alloy and soda lime glass. As shown in Figures 1(a_1) and (b_1), the surfaces of glass and metal are well cleaned without visible impurities such as dust, fingerprints, or other defects. The glass and metal surface morphology were observed using white light interferometer (BRUKER WYKO Contour GT-K). Figures 1(a_2) and Figure 1(b_2) are the 3D morphologies of Kovar alloy and glass surface before welding, respectively. The surface of Kovar alloy is relatively rougher. Glasses have been purchased with $\lambda/4$ flatness. The surface roughness R_a of Kovar alloy was 0.839 μm, which is rougher than the polished surfaces used for the previous study on glass-Al welding [20] (R_a of Al<100 nm), glass-aluminum welding [17] (R_a of aluminum 288 nm), glass-copper welding [21] (R_a of copper 210 nm). Therefore, in this paper, the welding of glass and Kovar alloy was not optically contacted.

2.2 fs laser welding equipment

The fs laser welding system was composed of a femtosecond fiber laser (FemtoYL-20, Wuhan Anyang Laser Technology Co., Ltd., China), a mirror system (Mirror 1-3), 10× Mitutoyo microscope objective lens (MY10×−823, THORLABS), a CCD vision system and a 3D Table, as shown in Figure 2. The experiment is performed using the femtosecond laser of 1030 nm wavelength, the adjustable pulsewidth of 200 − 1000 fs, and the maximum

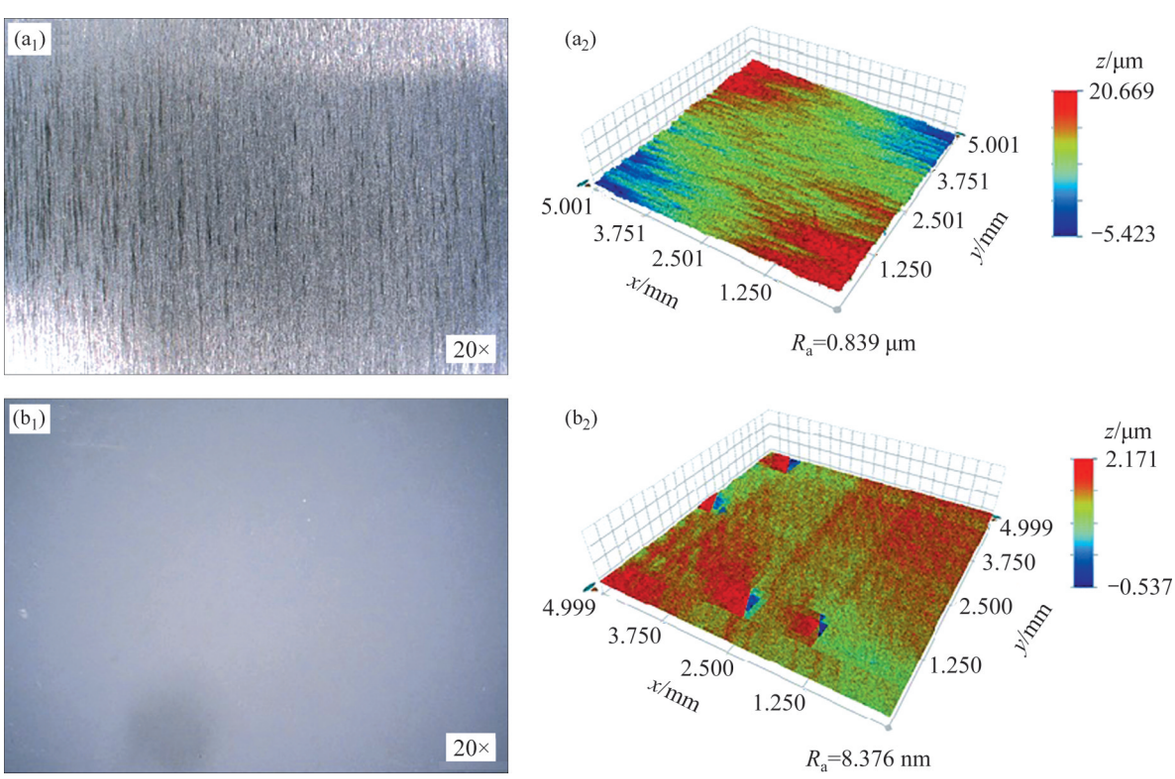

Figure 1 Initial surface states of Kovar alloy and soda lime glass: (a_1) Optical micrograph of Kovar alloy surface; (a_2) Kovar alloy surface roughness measured using white light interferometer; (b_1) Optical micrograph of soda lime glass surface; (b_2) Soda lime glass surface roughness measured using white light interferometer

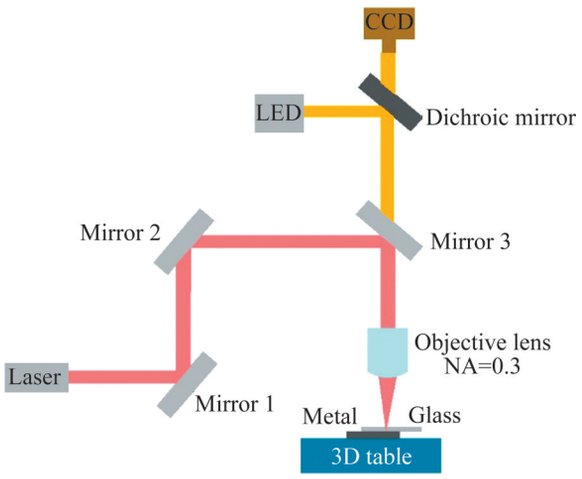

Figure 2 Schematic diagram of the optical path of fs laser welding system

output power of 20 W. And the repetition frequency of the laser can be adjusted within the range 0.025−5 MHz, while its single pulse energy remains unchanged. The samples were mounted onto a computer-controlled *XYZ* motion stage that allows translation parallel or perpendicular to the laser propagation axis. In order to focus the laser on the interface between 1 mm thick soda lime glass and 0.5 mm thick Kovar alloy, the THORLABS Mitutoyo flat field extinction near-infrared (NIR) object is used. The laser pulse, with a Gaussian intensity profile, was focused on the interface closer to the Kovar alloy surface through a long-working distance 10×Mitutoyo microscope objective (working distance 30.5 mm, nominal numerical aperture NA 0.3). It provides a flat focusing surface and chromatic aberration correction in the visible range, and maintains a long working distance between the lens surface and the samples, providing a good advantage for laser focusing.

The schematic diagram of sample cutting and observation is shown in Figure 3(a). As shown in Figure 3(b), the welding area is a square of 5 mm× 5 mm and the interval between the centers of adjacent welding lines is 200 μm. After the glass and Kovar alloy are cleaned, focus a fs laser on the glass and metal interface. The glass and Kovar alloy were initially pre-welded at a slower speed and lower energy to narrow the gap between glass and metal. Then the lap joints were successfully implemented by increasing the speed and the energy repeated scanning. After setting the appropriate

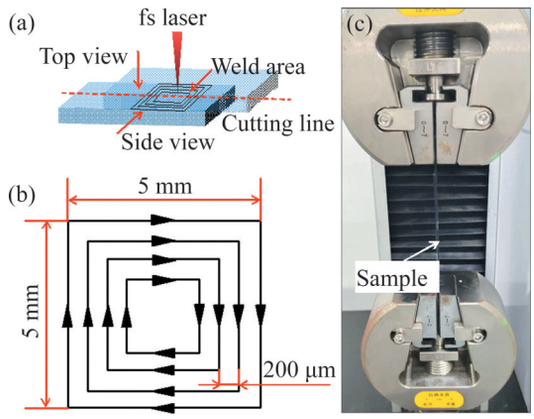

Figure 3 Welding process and tensile test setup: (a) The sample setup; (b) Welding path; (c) Shear tensile test

laser parameters, control the *Y*-axis to start to accelerate. When the preset speed is reached by acceleration, the laser emits light, which completes the glass-metal welding by scanning the square (Figure 3(b)). Before the uniform scanning is finished, the laser is turned off to eliminate the influence of platform acceleration and deceleration on welding quality. The schematic diagram of the universal tensile testing machine (KL-WL-2S) used for testing the shear joining strength is sketched in Figure 3(c). The shear joining strength was the critical thrust force which could separate the glass from the metal divided by the welding area. Various characterization methods, including universal tensile testing machine (KL-WL-2S), Keyence microscope (Keyence VHX-950F), scanning electron microscopy (SEM) and energy dispersive spectrometry (EDS) (Apreo 2 SEM) and white light interferometer (BRUKER WYKO Contour GT-K) were used in this work.

3 Results and discussion

3.1 Optimization of glass-Kovar alloy welding process

In order to further simplify the process and promote the industrial application of glass-metal welding by ultra-fast laser, as shown in Figure 3, the soda lime glass and Kovar alloy without optical contact are directly welded together by the fs laser welding system. This method was investigated to overcome the limit of optical contact. The welding results are shown in Figure 4(a). A welded region with a size of 5 mm×5 mm was formed by square

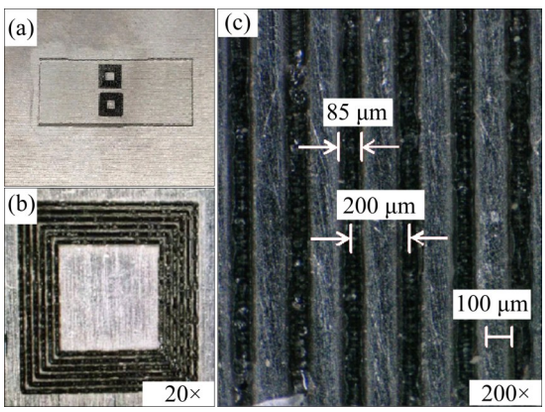

Figure 4 Optical microscope images of the samples after welding: (a) Soda lime glass and Kovar alloy without optical contact are directly welded together by fs laser; (b) Top view of the whole weld area (20× magnification); (c) Zoom-in of the welding line (200× magnification)

welding lines, as shown in Figure 4(b). Cracks are not found within the irradiated region. Figure 4(c) showed that the width of the welding line was about 85 μm. The interval between the centers of adjacent welding lines is about 200 μm.

The samples after post-joining separation are characterized using the Keyence microscope. The OM image of the welding seam on the soda lime glass surface is shown in Figure 5(a). A larger version of the Kovar alloy residuals is given in the upper right corner of Figure 5(b). Considerable Kovar alloy residuals in a dark color remained on the soda lime glass surface after shear-force separation as shown in Figure 5(a), revealing that a strong bonding strength has formed between glass and Kovar alloy for non-optical contact, which indicates that a sound joint is formed between soda lime glass and Kovar alloy in the irradiated area.

Next, the welding processing without optical

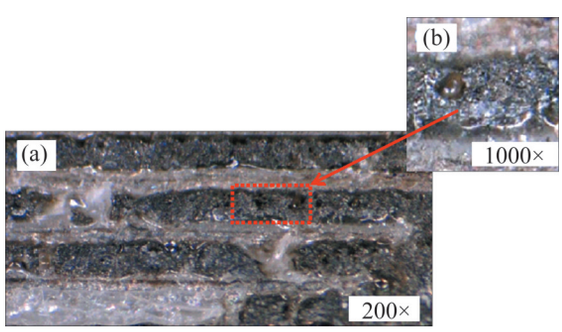

Figure 5 (a) Top view of the welding path (200× magnification); (b) Amplification of the red region (1000× magnification)

contact is optimized by varying the laser power, welding velocity, and the number of welding. Figure 6(a) shows the dependence of shear joining strength on laser power. For the energy scaning, the welding velocity was fixed at 1 mm/s. With the increased in laser power, the shear strength first increases and then decreased, and the shear strength reached the maximum value (2 MPa) when the laser power was 4.5 W. Experimental studies have shown that appropriately increasing the peak power density of laser irradiation can effectively improve the nonlinear absorption efficiency [22 – 23]. However, it is not advisable to blindly increase the peak power just to improve the energy absorption efficiency, since the too high peak power density can easily cause thermal damages, thermal stress residuals, and even micro-nano porous micro-structures in the laser action area [24 – 28]. The microstructure of weld joints with different laser processing

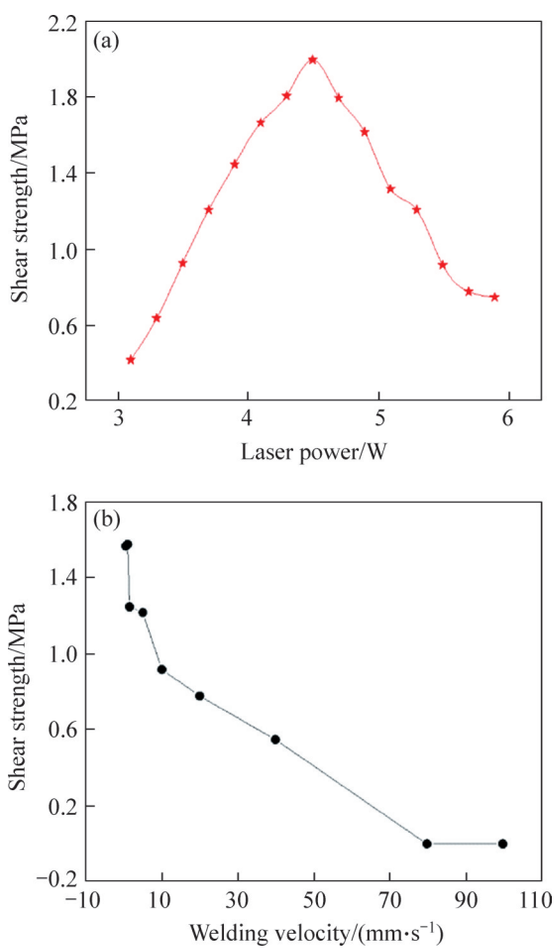

Figure 6 Influence of laser power and welding speed on the shear strength of joints: (a) Dependence of laser power parameters on shear strength; (b) Dependence of welding velocity on shear strength

parameters are shown in Figures 7(a)−(c). With the gradual increase of power, the black bonding layer formed by fs laser welding will gradually thicken and strengthen. However, the high power density will affect the absorption of glass and metal, and form cracks. It can be explained that the laser power for transmission welding reaches above 4.5 W, a shock wave is generated at the center of the focus; as the power density of the material at the center of the weld decreases, the power density of the surrounding material increases, a process of forming holes, splashing out the molten material, and producing cracks. Furthermore, an excessively high peak power density will result in the cold ablation of the sample interface, which will be detrimental to sample welding.

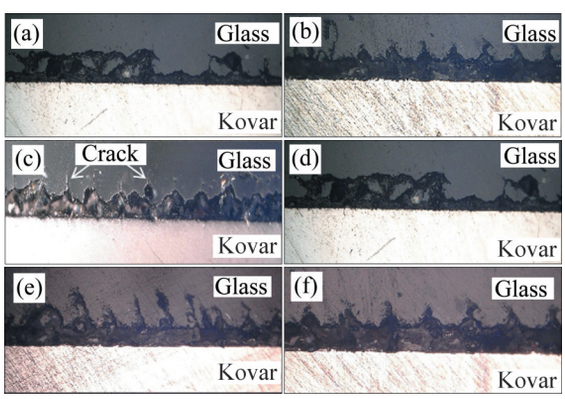

Figure 7 Microscopic appearance of welded joints under different process parameters: (a) P=4.1 W; (b) P=4.6 W; (c) P=5.1 W; (d) V=1 mm/s; (e) V=5 mm/s; (f) V=10 mm/s (P is the laser power and V is the welding velocity)

Figure 6(b) shows the shear strength of the joint at different welding velocity and a power of 4.1 W. It could be seen that the shear joining strength monotonously decreases with the increase of welding velocity in the range of 0.5 mm/s to 100 mm/s. The laser welding velocity also has an important influence on the quality of the joint. When the welding velocity exceeds 40 mm/s, the shear strength is insufficient to maintain the sample together as a whole. When the welding velocity is too low, there appears obvious ablation on the upper surface of the glass sample, which leads to the formation of cracks on the glass. On the contrary, a too high welding velocity could result in the base metal not being fully melted, hence the failure to form a high-quality weld. As shown in Figures 7(d)−(f), with the gradual increase of welding velocity, the escape of plasma will slightly decrease and then increase, and the welding strength will gradually decrease. When the welding velocity exceeds 80 mm/s, the welding will fail. It can be seen from the figure that the faster the welding velocity, the less the splashes.

Heat input will change, depending on the number of welding, which will make a difference to the welding quality. The term “number of welding” refers to the number of repeated processing of the welding pattern by the fs laser, which directly affects the fs-laser absorbed by the material. Welding around only 1 time will occur due to the insufficient heat input, the weld is not tightly and not firmly connected enough. With the increase in the number of welding, the heat input at the same position increases, and the material is more tightly and firmly welded. The black bonding layer with different numbers of welding is shown in Figure 8. As shown in Figures 8(a)−(c), when the number of welding is 1, 3 and 5, the thickness of the black bonding layer is 16 μm, 25 μm, 51 μm, respectively. It could be seen that the thickness of the black bonding layer increases with the number of welding in the range of 1 to 7. As shown in Figure 8(d), when the number of welding is 7, serious cracks and splashes will occur at the joint. However, too large number of welding and too much heat input will lead to cracks. Therefore, it is very important to find an appropriate number of welding and heat input. According to the microstructure of the weld joints with different number of welding in Figure 8, for 5 times of welding, the thickness of the black bonding layer is the largest; the plasma escape is the least; and the joint strength is the highest.

The experimental results show that the maximum shear strength can reach 2 MPa with one

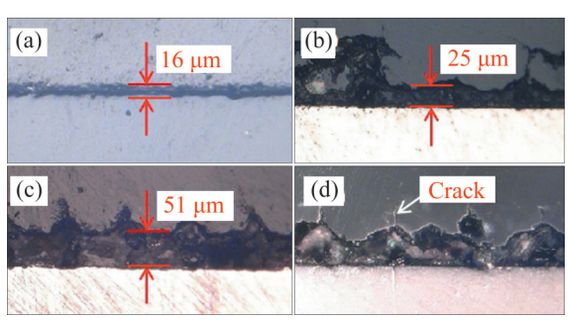

Figure 8 Microstructure of joints with different numbers of welding: (a) 1; (b) 3; (c) 5; (d) 7

pulse and at the laser power of 4.5 W, the repetition frequency of 0.1 MHz, the pulsewidth of 300 fs, and the constant welding velocity of 1 mm/s. For comparison, the shear strength described in an earlier study [19] was found to be 2.29 MPa for welding between the glass and polished copper. It is believed that we can implement the same order of magnitude of strength without polishing metal surface.

3.2 Cross-section of glass-Kovar alloy joints

The joint interface morphology of the welded samples was observed, in order to analyze the glass and Kovar alloy weld joints. Figure 9 shows the cross section of weld area observed by optical microscope after cutting, polishing and etching with hydrofluoric acid. The viewing directions are shown in Figure 3(a). The internal gap between the materials is obviously eliminated following fs laser irradiation, as illustrated in Figure 9(a). High peak power causes a series of nonlinear absorptions of glass after the fs laser is focused on the interface of glass and Kovar alloy. The instantaneous heat generated in a relatively closed space is difficult to diffuse, resulting in the melting and even gasification of materials at the focus region. After the molten glass and Kovar alloy are combined with each other, a black bonding layer as shown in Figure 9(a) is formed. As shown in Figure 9(a), the average width of black bonding layer is measured to be about 51.81 μm, which would be expected to have considerably increased the mechanical strength of the joint. Figure 9(b) is the larger version of black box area of Figure 9(a). The region marked in red is a black reaction layer, as illustrated in Figure 9(b), and the weld is generally continuous. When the fs laser irradiates the surface of Kovar alloy, micro/nanometer-sized metal particles are generated in the focus region. These particles then quickly melt and fuse with the molten glass, forming a black bonding interface between the glass and the Kovar alloy. These particles perform the role as an adhesive part in the welding process. Figure 9(c) is the larger version of green box area of Figure 9(a). Without the aid of clamp pressure, part of the plasma escape during the welding process is inevitable. As soon as the plasma diffuses too much to the outside of the molten pool, it will lead to a decrease in the

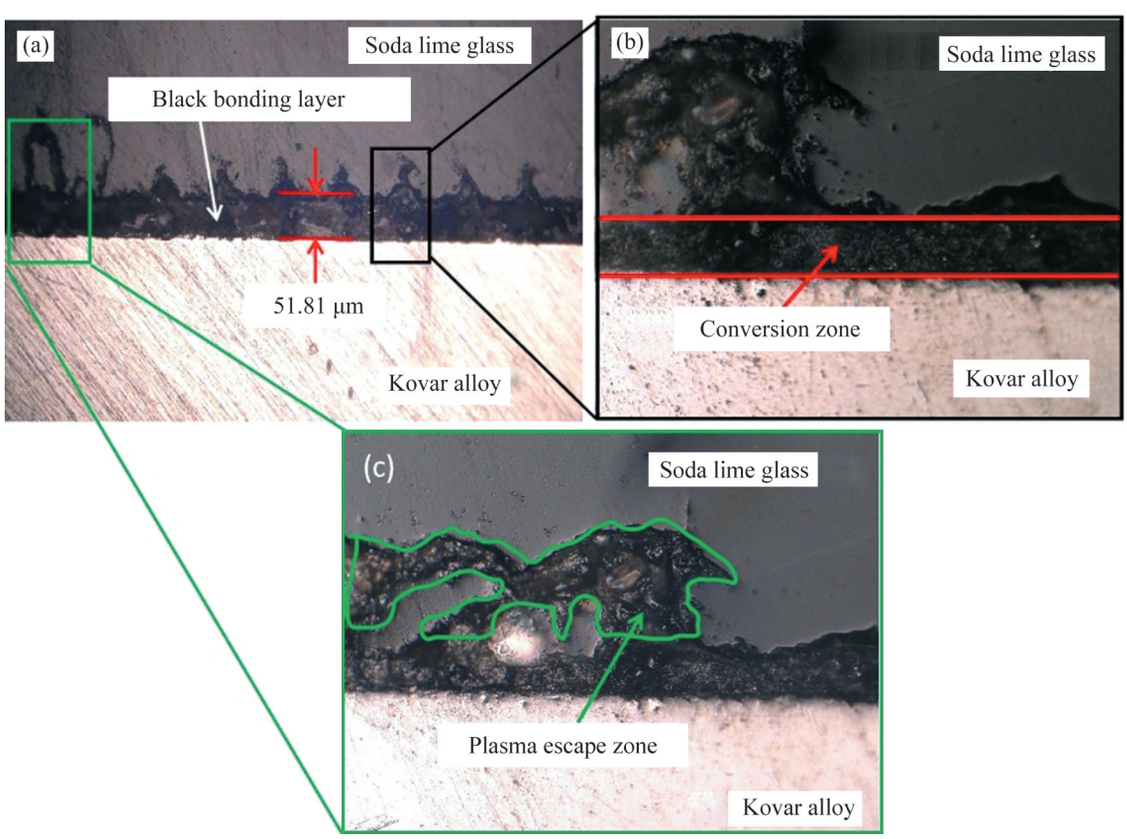

Figure 9 Cross-section of weld area: (a) Black bonding layer (side view); (b) Conversion zone (amplification of the black box area in (a)); (c) Plasma escape zone (amplification of the green box area in (a))

combination of the molten zone. The region marked in green in Figure 9(c) represents the plasma escape area. The formation mechanism of the plasma escape zone will be analyzed in detail in Section 3.5.

3.3 Elemental diffusion behavior analysis of weld joint

The morphology and chemical composition of cross-section of the welded sample is characterized. Figure 10 shows the cross section of weld area observed by SEM after cutting, polishing and spraying gold. The viewing directions are shown in Figure 3(a). As shown in Figure 10(a), a large number of black adherents were observed between the interface of glass and Kovar along the scanning direction. A small-sized interlock effect may be formed, resulting in a strong joining effect. Since the fs laser pulsewidth is far less than the thermal diffusion time of the material, the heat diffusion is negligible during the entire duration of the laser, affecting only a small zone, so there are very few microcracks during the welding process. As shown in Figure 10(b), there are irregular junction line at the bonging of glass and Kovar alloy joints, and the bonding lines are inlaid structures or transition layers formed by reaction. This indicates that the materials mixed and diffused during the laser irradiation of glass and metal. Next, the elemental distribution within the cross section of welding line is obtained by surface analysis with EDS as shown in Figure 11. As shown in Figure 11(a), the main elements in the welding area are Fe, Ni, Co, Si and O, with a small amount of Na and Mg. As shown in Figures 11(b)–(d), the distribution of O, Si, Fe on the surface of the glass-Kovar alloy joint. A transition layer can be observed between the distribution of Fe element and the distribution of O and Si elements in the glass. At the same time, the distribution of Fe element exists in the right part of the left layer boundary, whereas the O and Si elements of the glass exist in the left part of the right layer boundary. Elemental diffusion occured at the weld interface between the soda lime glass and Kovar alloy. This indicates that mixing and interdiffusion of materials have occurred during laser irradiation. The metallic oxide Fe_3O_4 on the surface of Kovar alloy, namely $Fe_2^{3+}Fe^{2+}O_4$, is a kind of spinel structure material, formed by the composite of FeO and Fe_2O_3. TU et al [29] introduced that due to the selective absorption of glass and Kovar alloy under 1030 nm wavelength laser, the laser beam acts directly on the oxide layer on the surface of Kovar alloy through the glass, leading to the following Reactions (1) and (2). TIE et al [30] found that Fe_3O_4 and Fe_2SiO_4 have similar crystal structures, and the Si atoms can be considered to enter the surface of Fe_3O_4 of Kovar alloy and partially replace the Fe^{2+} ions, leading to the formation of Fe_2SiO_4 with physical and chemical changes of the soda lime glass and Kovar alloy. It is believed that the mixed material near the interface acts as a buffer, which could effectively solve the mismatch of thermal expansion and melting points between glass and Kovar alloy. This is one of the main reasons why glass and Kovar alloy can achieve reliable bonding.

$$2Fe_3O_4+3SiO_2 \rightarrow 3Fe_2SiO_4+O_2 \quad (1)$$

$$2FeO+SiO_2 \rightarrow Fe_2SiO_4 \quad (2)$$

3.4 Fracture behavior analysis of welded joints

The fracture morphology of the welded sample

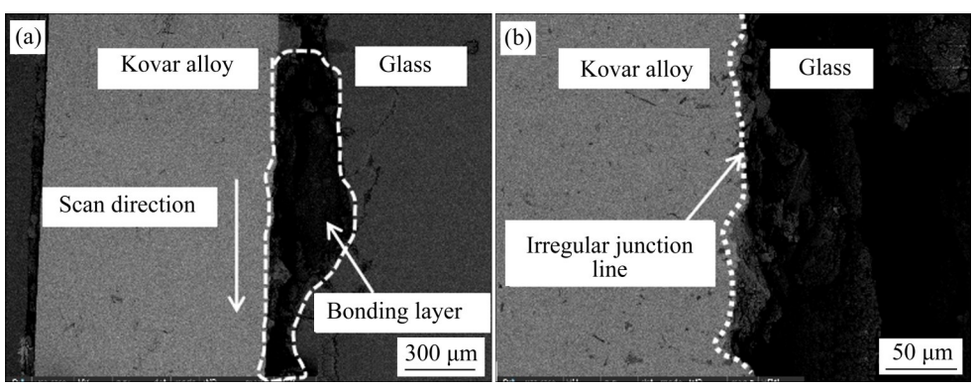

Figure 10 Morphology of the glass-Kovar alloy welding joints interface: (a) Cross section of welding area observed by SEM (side view); (b) Irregular junction line

joints is observed at a welding velocity of 1 mm/s and a laser power of 4.6 W, as shown in Figure 12, and the element distribution in each area is analyzed by EDS. The SEM diagram of partial fracture of the weld is shown in Figure 12(a). It can be seen that the glass and Kovar alloy have not fully melted together, but formed a thin new transition layer on their surfaces, after being welded by the fs laser.

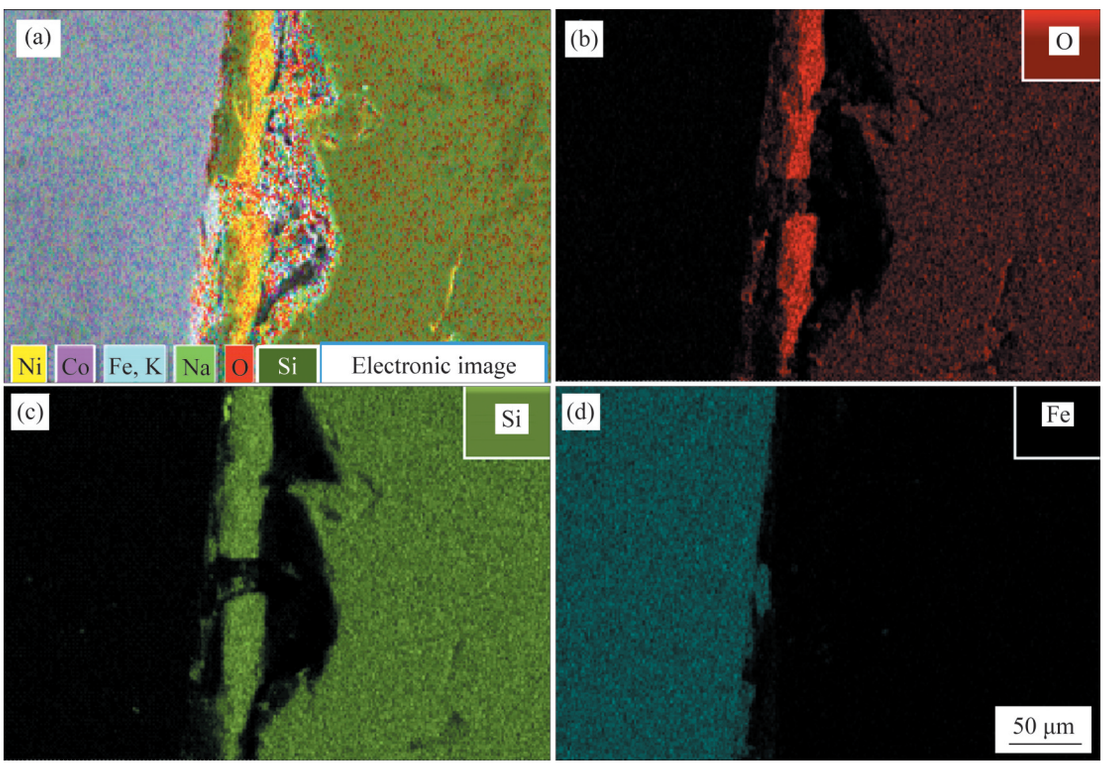

Figure 11 (a) SEM image of a typical central main weld bead cross-section and corresponding elemental distribution maps for (b) O, (c) Si and (d) Fe

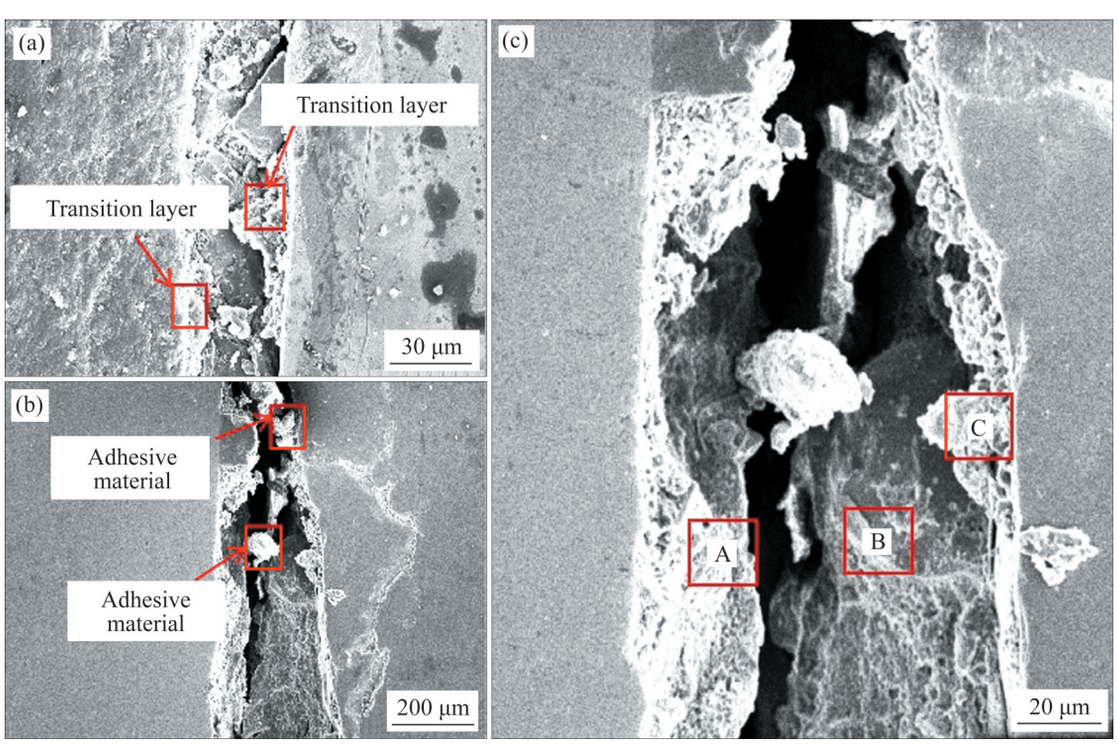

Figure 12 SEM images of weld fracture with different fracture degrees (side view): (a) Initial fracture of weld; (b) Weld fracture; (c) Amplification electron microscopy of fracture morphology of joint

The SEM images after the complete fracture of the weld are shown in Figure 12(b). After the separation of soda lime glass from Kovar alloy, there are still particles on the surface of glass and Kovar alloy. These micro/nano-sized particles can be considered as an adhesive part in the welding process, an indication of the high welding quality. As shown in Figure 12(c), the fracture morphology of the glass-Kovar alloy joints can be divided into three zones A, B and C. It can be seen from the SEM images after the weld fracture that the fracture in this zone occurs in the interface reaction zone between the glass and the oxide layer and at the junction between the oxide layer and the metal matrix.

3.5 Mechanism of microwelding and formation of plasma escape zone

In dissimilar material bonding, where only one material is transparent to the incident radiation, the fs laser lies in the combination of severely restricted thermal zones and the ability to trigger both nonlinear absorption in the transparent material and linear absorption in the opaque material. As shown in Figures 9(a) and (b), this generates a small heated zone around the interface forming of high temperature plasma in both materials simultaneously. As the plasma mixes and cools, a sound weld is formed. As seen in Figure 13, when a fs laser pulse is focused on glass-Kovar alloy interface, it triggers nonlinear absorption in the glass, which contributes to the generation of plasma in the focal region. ZHANG et al [8] introduced that when the fs-laser focus on the interface of two materials, the high-energy laser of the focus induces multiphoton ionization in glass, the speed of the ionizing free electrons increases by absorbing laser photon energy, and the electrons collide with other atoms, producing avalanche ionization. The electron-photon coupling raises the temperature of ionized and unionized parts to the melting point of the material, thereby completing the weld. As shown by the blue arrow in Figure 14, when the fs laser is irradiated on the glass, multiphoton ionization will occur. In this process, the electron-lattice coupling can be ignored. Within a few femtoseconds, the electrons transfer their energy into the crystal lattice, affecting the thermal equilibrium in the focal region through expansion, melting, phase change, and plasma evolution. Following that, local melting occurs at the interface between the transparent and opaque materials around the focal region, and the molten material resolidifies to bond the two materials. Finally, a black bonding layer is formed between the glass and the Kovar alloy.

As shown in Figure 9(c), the high temperature plasma was formed after fs laser irradiation impacts the glass material near the focusing zone, and sprayed out of the molten pool. Some of these plasma sprays were coincidently condensed into particles, resulting in the formation of a plasma escape zone. As shown in Figure 14, the brown arrow indicates the escape of plasma, and the blue arrow indicates the generation of multiphoton

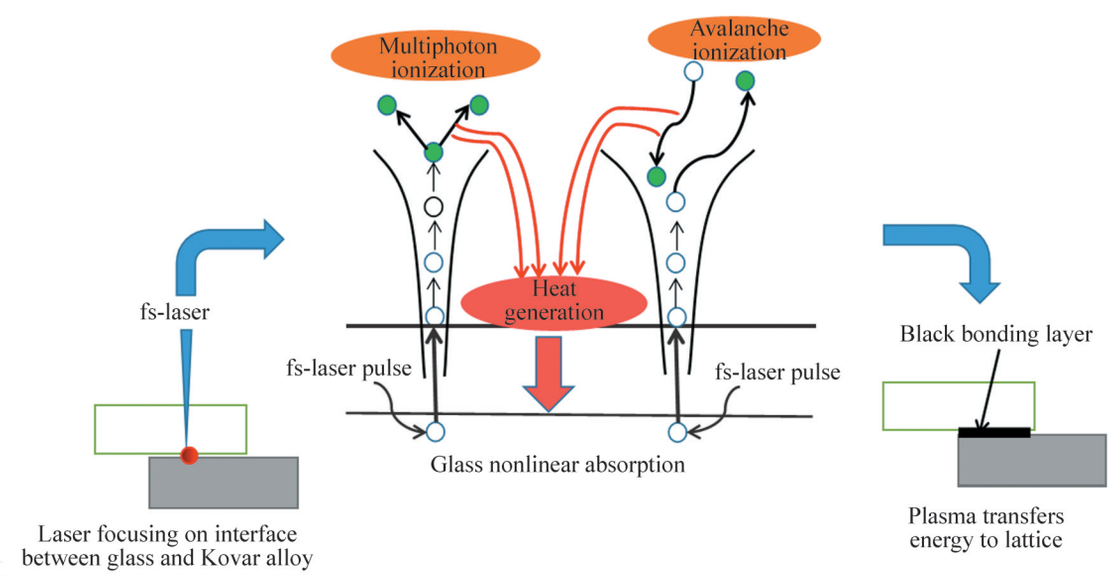

Figure 13 Mechanism of microwelding of fs laser

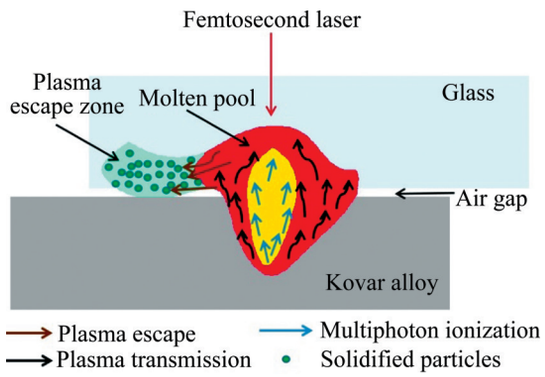

Figure 14 Formation mechanism of plasma escape zone (The air gap represents the without-optical contact part)

ionization. The black arrow indicates the plasma transmission in the molten pool, and the green sphere indicates the solid particles after melting and cooling. The air gap represents the without optical contact part. The mechanism of formation of the plasma escape zone is explained as follows: During the fs laser welding of glass and Kovar alloy, a mixture of droplets and gas is ejected from the molten pool, forming a particle distribution after cooling in the focal area. Since no clamping fixture is used in this experiment, partial plasma escape has resulted from the welding area. The plasma escape zone is formed after high temperature plasma impacts the glass material near the focus area. As shown in Figure 9(c), the outer surface of the irregular plasma escape area, which is extremely smooth without pits, is where molten glass flows and solidifies. When the liquid flows outward, the splashed liquid drops onto the liquid layer and cools rapidly, forming a large number of solidified particles. Still, many irregular solid particles have taken shape with the condensation of vapor-particle mixture outside. These solid particles cool and condense into a plasma escape zone.

3.6 Welded sample sealing test results

With the laser power of 4.1 W and welding speed of 1 mm/s, two sealing test samples were welded in the closed form: one was rectangular and the other was circular,as shown in Figures 15(a) and (b), respectively. Figures 15(c) and (d) are optical microscope images of the welding area of rectangular seal weld sample and ring seal weld sample, respectively. The sealing performance are tested by placing the welded samples in a solution

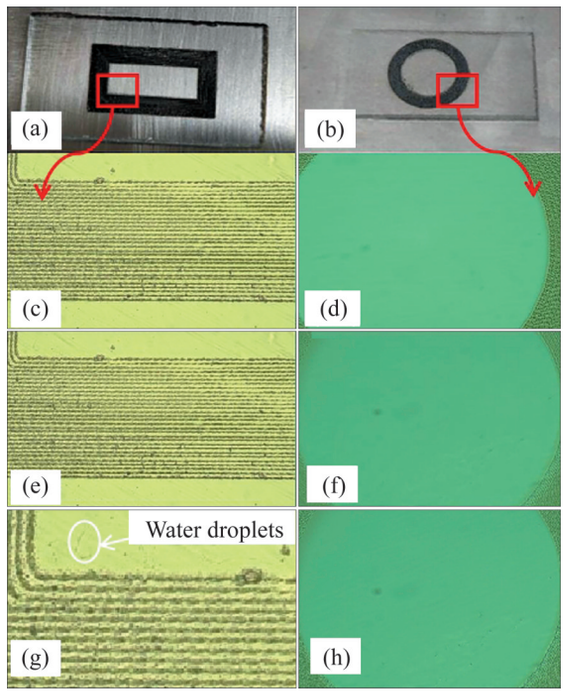

Figure 15 (a) Rectangular seal weld sample; (b) Ring seal weld sample; (c) Optical microscope images of rectangular seal weld sample; (d) Optical microscope images of ring seal weld sample; (e) Optical microscope images of rectangular seal of the sample in water for 2 h; (f) Optical microscope images of ring seal of the sample in water for 2 h; (g) Optical microscope images of the rectangular seal of the sample in water for 72 h; (h) Optical microscope images of ring seal of the sample in water after one week

with a ratio of carbon red ink to water of 1∶1. As shown in Figures 15(e) and (f), after 2 h, it was observed under the microscope that almost no red liquid infiltrated into the sealing zone, and the transparency of the non-welding area in the middle of the ring is also very good. No change occurs in sealing area before and after immersion in water. This indicates that two kinds of seal welding shapes have good sealing performance. As shown in Figure 15(g), after more than 72 h, the sample of rectangular seal ring began to infiltrate water into the sealing zone from the corner. As shown in Figure 15(h), the sample of the circular seal ring could still maintain good sealing performance after one week in water. CHEN et al [31] established that the reason for the poor sealing effect of the rectangular seal weld is that more energy is deposited, hence greater stress, at its corner under the same fs laser welding parameters. Unevenly

distributed stress on the rectangular seal weld can easily lead to fracture of the corner of glass, so its samples cannot maintain good sealing effect for a long time. However, the samples of the circular sealing weld have good consistency and can obtain uniform stress distribution on the welding path, hence good sealing performance.

As a functional material, Kovar alloy has similar expansion coefficient to that of glass over a large temperature range (−80 °C−450 °C), ensuring the material's matching sealing. Since Kovar alloy and glass have similar coefficient of thermal expansion, this may be one of the reasons why a clamping is not required. In order to verify that this method is also applicable to other materials, glass-copper, glass-Al6063, and glass-ceramic with large differences in coefficient of thermal expansion were successfully welded together, as shown in Figure 16. This shows that the method is also suitable for welding other dissimilar materials.

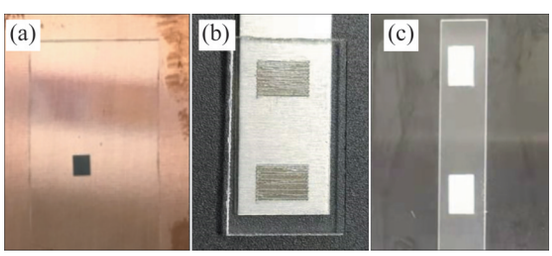

Figure 16 Welding of glass and other materials: (a) Soda lime glass-copper; (b) Soda lime glass-Al6063; (c) Sapphire glass-ceramic

4 Conclusions

In this paper, direct microwelding of soda lime glass and Kovar alloy using a 1030 nm fs laser is successfully implemented without optical contact. This method overcomes the limitation of optical contact and simplifies the welding process. Welded samples have been obtained with good sealing performance and the shear strength up to 2 MPa. The circular seal ring has outperformed the rectangular seal ring in the water sealing test. The morphology, the formation of plasma escape zone, tensile-fracture mode, the elements diffusion of the welded joint were studied. The following conclusions were drawn:

1) When the fs laser irradiates the surface of Kovar alloy, micron/nanometer-sized metal particles are generated. These particles perform the role as an adhesive part in the welding process.

2) The high temperature plasma was formed after fs laser irradiation impacts the glass material near the focusing zone, and sprayed out of the molten pool. Some of these plasma sprays were coincidently condensed into particles, resulting in the formation of a plasma escape zone.

3) Elemental diffusion occurred at the weld interface between the soda lime glass and Kovar alloy, which is an important reason for the formation of high-strength welded joints. When the laser power for transmission welding was high, the Kovar alloy is ablated due to excessive energy input, and the glass was cracked, thus reducing the welding strength.

4) The technique of fs laser microwelding can be applied to other stack ups without surface polishing or pressure fixture assistance, such as the glass-copper, the glass-Al6063 and sapphire-ceramic.

This work proves that the current requirements on roughness and cleanliness of the material surface could be relaxed. In the future, since the focused objective lens used in this work has limited scanning speed, it will be interesting to explore the effect of the welding speed, also the effects of the surface texture, the microstructure of metal and glass, and the welding environment, such as underwater, vacuum, and different atmospheres on the joint strength.

Contributors

The overarching research goals were developed by LONG Yu, JI Chang-hao, and HUANG Yu-jia. JI Chang-hao provided the concept, conducted the literature review and wrote the first draft of the manuscript. JI Chang-hao, CHEN Xu and JIANG Ji-yan analyzed the measured data. LONG Yu, HUANG Yu-jia, CHEN Xu, JIANG Ji-yan and GUO Zhi-jun edited the draft of manuscript. All authors replied to reviewers' comments and revised the final version.

Conflict of interest

The authors declare that they have no known competing financial interests or personal relationships that could have appeared to influence the work reported in this paper.

References

[1] YI Rui-xiang, CHEN Chao, LI Yu-xiang, et al. The bonding between glass and metal [J]. The International Journal of Advanced Manufacturing Technology, 2020, 111(3−4): 963−983. DOI: 10.1007/s00170-020-06018-x.

[2] SHI Chen, YI Rui-xiang, CHEN Chao, et al. Forming mechanism of the repairing process on clinched joint [J]. Journal of Manufacturing Processes, 2020, 50: 329 − 335. DOI: 10.1016/j.jmapro.2019.12.025.

[3] PETHRICK R A. Composite to metal bonding in aerospace and other applications [M]// Welding and Joining of Aerospace Materials. Amsterdam: Elsevier, 2012: 288 − 319. DOI: 10.1533/9780857095169.2.288.

[4] KIM S, PARK J, SO S, et al. Characteristics of an implantable blood pressure sensor packaged by ultrafast laser microwelding [J]. Sensors (Basel, Switzerland), 2019, 19(8): 1801. DOI: 10.3390/s19081801.

[5] CHOU Y S, STEVENSON J W, SINGH P. Effect of pre-oxidation and environmental aging on the seal strength of a novel high-temperature solid oxide fuel cell (SOFC) sealing glass with metallic interconnect [J]. Journal of Power Sources, 2008, 184(1): 238 − 244. DOI: 10.1016/j. jpowsour. 2008.06.020.

[6] HÉLIE D, GOUIN S, VALLÉE R. Assembling an endcap to optical fibers by femtosecond laser welding and milling [J]. Optical Materials Express, 2013, 3(10): 1742. DOI: 10.1364/ome.3.001742.

[7] BRIAND D, WEBER P, DE ROOIJ N F. Metal to glass anodic bonding for microsystems packaging [C]// TRANSDUCERS '03.12th International Conference on Solid-State Sensors, Actuators and Microsystems. Digest of Technical Papers (Cat. No. 03TH8664). June 8 − 12, 2003, Boston, MA, USA. IEEE, 2003: 1824−1827. DOI: 10.1109/SENSOR.2003.1217142.

[8] ZHANG Jie-juan, XU Si-zhi, DONG Yu-kun, et al. Microwelding of glass to silicon by green ultrafast laser pulses [J]. Optics & Laser Technology, 2019, 120: 105720. DOI: 10.1016/j.optlastec.2019.105720.

[9] SUN Ke, SUN Sheng-zhi, Qiu Jian-rong. Research progress of ultrashort pulse laser welding nonmetallic materials [J]. Laser & Optoelectronics Progress, 2020, 11: 282−291. DOI: 10.3788/LOP57.111422. (in Chinese)

[10] FAN Wen-zhong, ZHAO Quan-zhong. Recent progress in ultrashort pulsed laser microwelding of glasses [J]. Laser & Optoelectronics Progress, 2015, 52(8): 7−19. (in Chinese)

[11] DING Teng, WANG Xue-hui, WANG Guan-de, et al. Welding of fused silica by using high repetition frequency femtosecond laser [J]. Chinese Journal of Lasers, 2018, 45(7): 46−52. (in Chinese)

[12] HUANG Huan, YANG L M, LIU Jian. Ultrashort pulsed fiber laser welding and sealing of transparent materials [J]. Applied Optics, 2012, 51(15): 2979 − 2986. DOI: 10.1364/AO.51.002979.

[13] KONGSUWAN P, SATOH G, YAO Y L. Transmission welding of glass by femtosecond laser: Mechanism and fracture strength [J]. Journal of Manufacturing Science and Engineering, 2012, 134(1): 011004. DOI: 10.1115/1.4005306.

[14] RICHTER S, ZIMMERMANN F, SUTTER D, et al. Ultrashort pulse laser welding of glasses without optical contacting [C]//SPIE LASE. Proc SPIE 10094, Frontiers in Ultrafast Optics: Biomedical, Scientific, and Industrial Applications XVII, San Francisco, California, USA. 2017, 10094: 118−125. DOI: 10.1117/12.2250389.

[15] OZEKI Y, INOUE T, TAMAKI T, et al. Direct welding between copper and glass substrates with femtosecond laser pulses [J]. Applied Physics Express, 2008, 1: 082601. DOI: 10.1143/apex.1.082601.

[16] QUINTINO L, LIU L, MIRANDA R M, et al. Bonding NiTi to glass with femtosecond laser pulses [J]. Materials Letters, 2013, 98: 142−145. DOI: 10.1016/j.matlet.2013.02.051.

[17] CARTER R M, TROUGHTON M, CHEN Jian-yong, et al. Towards industrial ultrafast laser microwelding: SiO_2 and BK7 to aluminum alloy [J]. Applied Optics, 2017, 56(16): 4873−4881. DOI: 10.1364/AO.56.004873.

[18] LAFON R E, LI S, MICALIZZI F, et al. Ultrafast laser bonding of glasses and crystals to metals for epoxy-free optical instruments [C]// SPIE LASE. Proc SPIE 11261, Components and Packaging for Laser Systems VI, San Francisco, California, USA. 2020, 11261: 1126103. DOI: 10.1117/12.2551503.

[19] ZHANG Guo-dong, CHENG Guang-hua. Direct welding of glass and metal by 1 kHz femtosecond laser pulses [J]. Applied Optics, 2015, 54(30): 8957 − 8961. DOI: 10.1364/AO.54.008957.

[20] CARTER R M, CHEN Jian-yong, SHEPHARD J D, et al. Picosecond laser welding of similar and dissimilar materials [J]. Applied Optics, 2014, 53(19): 4233−4238. DOI: 10.1364/AO.53.004233.

[21] MATSUYOSHI S, MIZUGUCHI Y, MURATSUGU A, et al. Welding of glass and copper with a rough surface using femtosecond fiber laser pulses [J]. Journal of Laser Micro/Nanoengineering, 2018, 13(1): 21 − 25. DOI: 10.2961/jlmn. 2018.01.0005.

[22] OUYANG Zhi-yong, OKAMOTO Y, OGINO Y, et al. Influence of numerical aperture on molten area formation in fusion micro-welding of glass by picosecond pulsed laser [J]. Applied Sciences, 2019, 9(7): 1412. DOI: 10.3390/app907 1412.

[23] MIYAMOTO I, CVECEK K, SCHMIDT M. Evaluation of nonlinear absorptivity in internal modification of bulk glass by ultrashort laser pulses [J]. Optics Express, 2011, 19(11): 10714−10727. DOI: 10.1364/OE.19.010714.

[24] KISSI E O, BELLOUARD Y. Self-organized nanostructures forming under high-repetition rate femtosecond laser bulk-heating of fused silica [J]. Optics Express, 2018, 26(11): 14024−14037. DOI: 10.1364/OE.26.014024.

[25] CVECEK K, MIYAMOTO I, SCHMIDT M. Gas bubble formation in fused silica generated by ultra-short laser pulses [J]. Optics Express, 2014, 22(13): 15877 − 15893. DOI: 10.1364/OE.22.015877.

[26] ZHANG Guo-dong, CHENG Guang-hua, BHUYAN M K, et al. Ultrashort Bessel beam photoinscription of Bragg grating waveguides and their application as temperature sensors [J]. Photonics Research, 2019, 7(7): 806. DOI: 10.1364/prj. 7.000806.

[27] ZHANG G, CHENG G, BHUYAN M, et al. Efficient point-by-point Bragg gratings fabricated in embedded laser-written

silica waveguides using ultrafast Bessel beams [J]. Optics Letters, 2018, 43(9): 2161 − 2164. DOI: 10.1364/OL.43.002161.

[28] STOIAN R, BHUYAN M K, ZHANG Guo-dong, et al. Ultrafast Bessel beams: Advanced tools for laser materials processing [J]. Advanced Optical Technologies, 2018, 7(3): 165−174. DOI: 10.1515/aot-2018-0009.

[29] TU Ye, JI Ling-fei, BAO Yong, et al. Joining behavior and interface analysis of Pyrex glass-to-KOVAR alloy with fiber laser [J]. Applied Laser, 2011, 31(1): 12−14. (in Chinese)

[30] TIE Min, LI Hong, LI Zhuo-xin, JIA Lin. Laser welding technology of borosilicate glass and Kovar alloy [J]. Transactions of the China Welding Institution. 2016, 37: 55−58, 74, 131. DOI: CNKI: SUN: HJXB.0.2016-06-013. (in Chinese)

[31] CHEN Hang, DUAN Jun, YANG Ze-qi, et al. Picosecond laser seal welding of glasses with a large gap [J]. Optics Express, 2019, 27(21): 30297−30307. DOI: 10.1364/OE.27.030297.

(Edited by ZHENG Yu-tong)

中文导读

非光学接触状态下玻璃和可伐合金异种材料的飞秒激光微连接

摘要：飞秒激光由于能有效避免热扩散、热损伤以及防止热应力产生裂纹和溅射物等优点而广泛应用于微纳米尺度材料连接领域。但目前使用飞秒激光焊接异种材料时，两种材料之间一般需达到光学接触。为了达到上述要求，通常认为材料表面抛光和压力辅助是必要的。本文使用飞秒激光直接焊接钠钙玻璃和可伐合金，克服了光学接触的限制。通过改变激光功率、焊接速度和焊接次数来优化焊接工艺参数。接头的剪切连接强度可到达2 MPa。利用基恩士显微镜、扫描电子显微镜(SEM)、能谱分析仪(EDS)分析了玻璃-可伐合金接头的截面、元素扩散行为和接头的断裂行为。结果表明，飞秒激光辐照金属材料表面后，会在表面产生微纳米级微小颗粒，这种微小颗粒可被认为是焊接过程中的粘合剂。焊接区硅和氧元素有明显的变化，玻璃表面的元素Si进入可伐合金表面，部分取代了可伐合金表面的Fe^{2+}，表明在激光照射过程中发生了物质的混合和相互扩散。同时也对飞秒激光焊接玻璃和可伐合金的过程中等离子体逃逸区的形成机制进行了分析。最后，对焊后样品进行了密封性测试，发现其具有良好的耐水性和密封性。为了证明这种方法可以应用于其他材料，玻璃-铜，玻璃-Al6063，蓝宝石-陶瓷也被焊接到一起。这项工作有望简化飞秒激光微焊接工艺，并促进其在工业上的应用。

关键词：飞秒激光；微连接；玻璃；可伐合金；光学接触